Neuroradiology (2021) 63:63–71
https://doi.org/10.1007/s00234-020-02513-w

DIAGNOSTIC NEURORADIOLOGY

A preliminary study of deep learning-based reconstruction specialized for denoising in high-frequency domain: usefulness in high-resolution three-dimensional magnetic resonance cisternography of the cerebellopontine angle

Hiroyuki Uetani[1] · Takeshi Nakaura[1] · Mika Kitajima[1] · Yuichi Yamashita[2] · Tadashi Hamasaki[3] · Machiko Tateishi[1] · Kosuke Morita[4] · Akira Sasao[1] · Seitaro Oda[1] · Osamu Ikeda[1] · Yasuyuki Yamashita[1]

Received: 17 June 2020 / Accepted: 4 August 2020 / Published online: 13 August 2020

Abstract

Purpose Deep learning-based reconstruction (DLR) has been developed to reduce image noise and increase the signal-to-noise ratio (SNR). We aimed to evaluate the efficacy of DLR for high spatial resolution (HR)-MR cisternography.

Methods This retrospective study included 35 patients who underwent HR-MR cisternography. The images were reconstructed with or without DLR. The SNRs of the CSF and pons, contrast of the CSF and pons, and sharpness of the normal-side trigeminal nerve using full width at half maximum (FWHM) were compared between the two image types. Noise quality, sharpness, artifacts, and overall image quality of these two types of images were qualitatively scored.

Results The SNRs of the CSF and pons were significantly higher with DLR than without DLR (CSF 21.81 ± 7.60 vs. 15.33 ± 4.03, $p < 0.001$; pons 5.96 ± 1.38 vs. 3.99 ± 0.48, $p < 0.001$). There were no significant differences in the contrast of the CSF and pons ($p = 0.225$) and sharpness of the normal-side trigeminal nerve using FWHM ($p = 0.185$) without and with DLR, respectively. Noise quality and the overall image quality were significantly higher with DLR than without DLR (noise quality 3.95 ± 0.19 vs. 2.53 ± 0.44, $p < 0.001$; overall image quality 3.97 ± 0.17 vs. 2.97 ± 0.12, $p < 0.001$). There were no significant differences in sharpness ($p = 0.371$) and artifacts ($p = 1$) without and with DLR.

Conclusion DLR can improve the image quality of HR-MR cisternography by reducing image noise without sacrificing contrast or sharpness.

Keywords Deep learning · Image reconstruction · Magnetic resonance imaging · Noise · Signal-to-noise ratio

Abbreviations

3D	Three-dimensional
DCT	Discrete cosine transform
DLR	Deep learning-based reconstruction
FASE	Fast asymmetric spin-echo
FWHM	Full width at half maximum
HR	High-spatial resolution
SNR	Signal-to-noise ratio
T1WI	T1-weighted image
T2WI	T2-weighted image
CNR	Contrast-to-noise ratio

✉ Hiroyuki Uetani
hama-moto@hotmail.co.jp

[1] Department of Diagnostic Radiology, Faculty of Life Sciences, Kumamoto University, 1-1-1 Honjo, Chuo-ku, Kumamoto, Japan

[2] Canon Medical Systems Corporation, MRI Sales Department, Sales Engineer Group, 70-1, Yanagi-cho, Saiwai-ku, Kawasaki-shi, Kanagawa 212-0015, Japan

[3] Department of Diagnostic, Neurosurgery, Faculty of Life Sciences, Kumamoto University, 1-1-1 Honjo, Chuo-ku, Kumamoto, Japan

[4] Department of Radiology, Kumamoto University Hospital, 1-1-1 Honjo, Chuo-ku, Kumamoto, Japan

Introduction

High-spatial resolution (HR) three-dimensional (3D) T2-weighted images (T2WIs) of the cerebellopontine angle have been used to evaluate cerebellopontine angle tumors [1], epidermoid cyst [2], neurovascular compression [3], arterial anatomy [4], and cranial nerve anatomy [5]. HR 3D T2WIs have

high diagnostic accuracy and inter-rater agreement for the evaluation of cerebellopontine angle lesions in patients with asymmetrical audiovestibular complaints, and these are comparable with those of contrast-enhanced 3D T1-weighted images (T1WIs) [6]. In addition, HR 3D T2WIs fused with 3D time-of-flight MR angiography are a reliable imaging tool with high inter-rater agreement for neurovascular compression [7]. However, this imaging technique has some problems, including a long scan time and decrease in the signal-to-noise ratio (SNR) [8]. A parallel imaging technique has been widely used to reduce the scan time [9, 10]; nonetheless, usage of this technique generally reduces the SNR. Recently, a compressed sensing technique has been introduced for clinical use to reduce the scan time and maintain the SNR [11]. In this technique, denoising methods, such as adoption of a Gaussian smoothing filter and iterative reconstruction with a wavelet filter, have been used to reduce noise and improve the SNR. However, some studies have reported that some sequences using this technique may have global ringing artifacts and blurring of fine details [12, 13]. Therefore, other techniques may present advantages for obtaining HR 3D T2WIs.

Recently, machine learning and deep learning techniques have been applied to radiological images and reported to be useful for lesion detection [14, 15], segmentation [16, 17], and classification [18, 19]. Furthermore, the usefulness of deep learning-based reconstruction (DLR) for denoising MRI images has been reported [20–22]. DLR denoising is a technology based on convolutional neural networks applied to image denoising and is fundamentally different from ordinary frequency-based methods in that machine learning is performed using noise and other discrimination factors among high-frequency components as training data. Therefore, DLR might reduce image noise without decreasing spatial resolution. However, to our knowledge, no report has evaluated the efficacy of DLR for HR-MR cisternography.

Therefore, the purpose of this study was to evaluate the efficacy of DLR for HR-MR cisternography.

Methods

One author (Y.Y.) is an employee of Canon Medical Systems. The other authors are not employees of or consultants for the industry. We used a commercial-based denoising technique with DLR and received no industry support or funding for this study. H.U. and T. N. had full control of all data and information submitted for publication.

This retrospective study was approved by our institutional review board. Informed consent for this retrospective study was waived by our institutional ethics committee.

Population

This retrospective study identified 37 consecutive patients who underwent head MRI, including HR-MR cisternography. Two patients with cerebellopontine angle tumors were excluded because we could not evaluate the trigeminal nerve according to the mass effect. Finally, we included 35 consecutive patients (9 men and 26 women; age range, 20–88 years; mean age, 53.7 ± 17.7 years) (Fig. 1). Of these 35 patients, 25 underwent MRI to evaluate known cerebellopontine angle tumors and 10 underwent MRI to rule out cerebellopontine angle tumors. (Seventeen patients [68%] had vestibular nerve schwannoma, 1 [4%] had trigeminal nerve schwannoma, 1 [4%] had accessory nerve schwannoma, 3 [12%] had meningioma in cerebellopontine angle, 1 [4%] had midbrain glioma, 1 [4%] had external acoustic meatus carcinoma, and 1 [4%] had cholesteatoma. Seventeen patients [68%] were preoperation study, and 8 patients [32%] were post-operation study. All 25 patients had unilateral lesion. Five [25%] patients had mass effect on the pons, 14 [56%] had cerebellopontine angle lesion, and 14 [56%] had internal auditory canal lesion. The mean tumor size was 17 mm [0–40 mm].) All images were acquired between October 2018 and April 2019.

MRI sequences and parameters

Brain studies were performed using a 3T MRI scanner (Vantage Galan 3 T ZGO; Canon Medical Systems) with a 32-channel head coil. After generating scout images, we obtained T1WIs, T2WIs, FLAIR images, diffusion-weighted images, and HR 3D isotropic T2-weighted fast asymmetric spin-echo (FASE) images of the cerebellopontine angle (HR-MR cisternography), which were recommended by the MRI vendor. The imaging parameters of HR-MR cisternography were as follows: repetition time, 2500 ms; echo time, 91.5 ms; inversion time, 180 ms; acquisition voxel size, 0.46 × 0.45 × 0.5 mm; reconstruction voxel size, 0.23 × 0.23 × 0.5 mm; number of excitations, 1; field of view, 210 × 180 mm; flip angle, 90°; number of sections, 100; section thickness, 0.5 mm; parallel imaging factor (SPEEDER), 2; and scan time, 5 min 40 s.

We performed HR-MR cisternography with and without DLR. Denoising DLR using deep convolutional neural networks was performed after converting k-space to real space with inverse fast Fourier transform [23]. DLR derives 49 components with a fixed 7 × 7 discrete cosine transform (DCT) basis. In 49 channels, the zero-frequency component of DCT follows a separate collateral path, whereas the other 48 high-frequency components are processed as feature maps in subsequent feature conversion layers. The zero-frequency component of a 7 × 7 DCT is equivalent to a 7 × 7 unweighted moving average filter. Separation of this zero-frequency

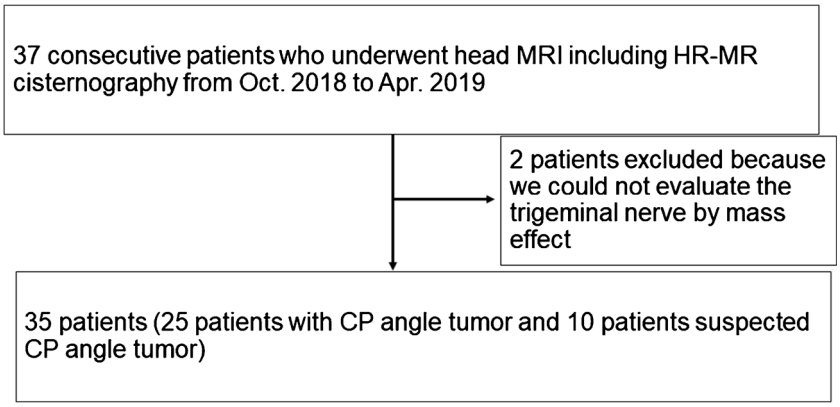

Fig. 1 Flow diagram shows patient inclusion criteria

component from the feature extraction layer allows the process to maintain image contrast. However, with the use of a 7 × 7 moving average filter, the edges of detailed structures are lost, similar to a low-pass image filter. Conversely, high-frequency components that include noise and detailed structures pass into the path of feature conversion layers. DLR with a separated path of high-frequency components can learn convolutional neural network parameters to remove noise and maintain detailed structures. After the denoising process, the denoised high-pass components and the zero-frequency component are combined. The architecture and schema of DLR are shown in Figs. 2 and 3, respectively. The algorithm of DLR used in this study is completely the same as the previous report by Kidoh et al. [22]. The final DLR images can be added to the original images to change the denoising intensity, and this ratio is called a DLR blend ratio. We used the blending ratio of 50% as recommended by the MRI vendor.

Quantitative image analysis

A board-certified neuroradiologist with 29 years of experience with MRI performed quantitative image analysis on the two types of HR-MR cisternography images. The slice level of the pons was selected. Signal intensity and standard deviation were measured by placing circular ROIs at the CSF and pons. The ROIs were at least 50 mm^2, and they were placed in homogeneous, artifact-free areas of the tissues. Image noise was defined as the standard deviation of the same ROIs for signal intensity because the background noise was too low. The SNR, contrast, and contrast-to-noise ratio (CNR) for HR-MR cisternography were calculated with or without DLR.

The SNR of the CSF/pons was calculated using the following formula: $SNR = mean\ signal\ intensity\ /\ mean\ standard\ deviation$. The contrast between the CSF and pons was determined using the following formula: $contrast\ ratio = (mean\ signal\ intensity_{CSF} - mean\ signal\ intensity_{pons})\ /\ (mean\ signal\ intensity_{CSF} + mean\ signal\ intensity_{pons})$. The CNR between

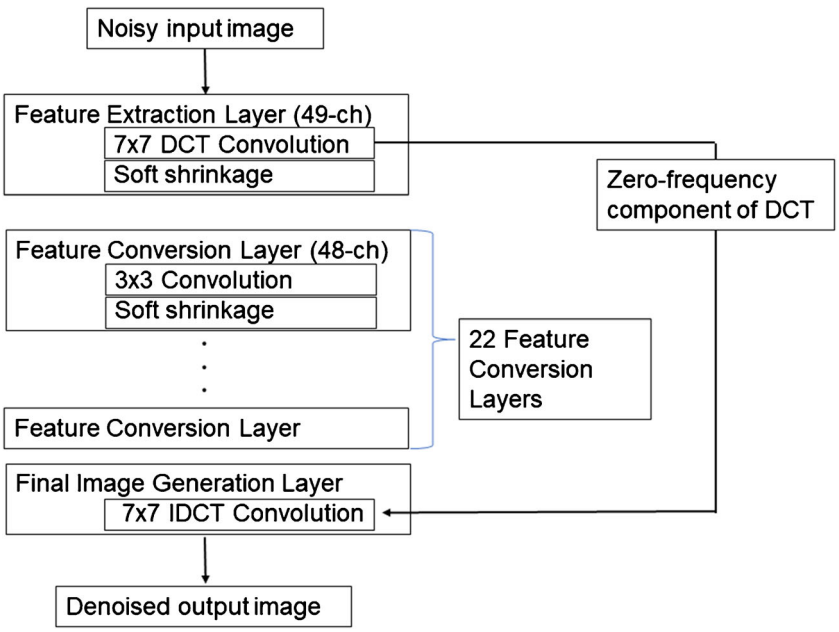

Fig. 2 Deep learning-based reconstruction (DLR) architecture. DLR derives 49 components with a fixed 7 × 7 discrete cosine transform (DCT) basis. In 49 channels, the zero-frequency component of DCT follows a separate collateral path, whereas the other 48 high-frequency components are processed as feature maps in subsequent feature conversion layers. DLR with a separated path of high-frequency components can learn convolutional neural network parameters to remove noise and maintain detailed structures. After the denoising process, the denoised high-pass components and the zero-frequency component are combined

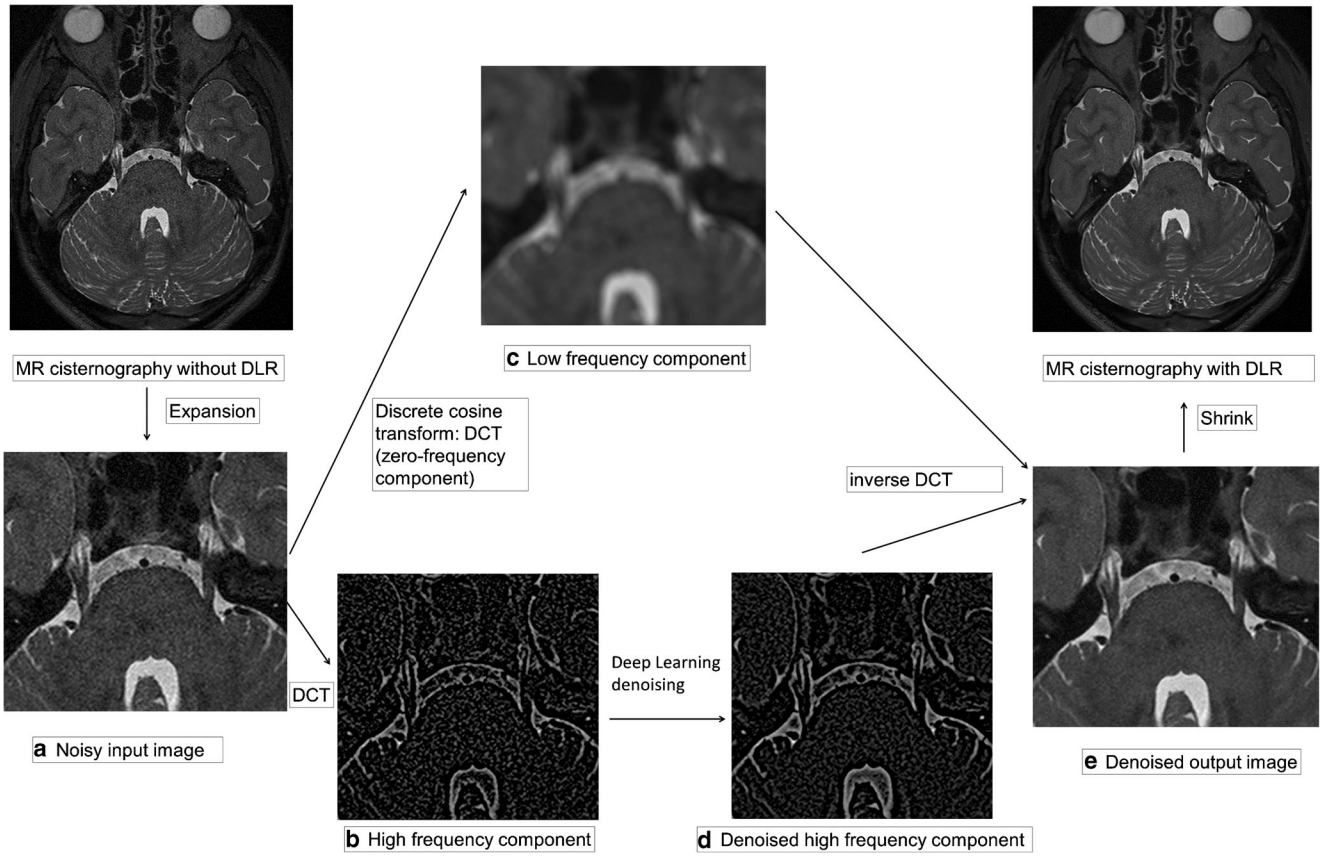

Fig. 3 Schema of the denoising process with deep learning-based reconstruction (DLR). Noisy input images (**a**) are divided into 49 high (**b**)- and low (**c**)-frequency components with a fixed 7 × 7 discrete cosine transform (DCT) basis. In 49 channels, the zero-frequency component of DCT (7 × 7 moving average filtered image) follows a separate collateral path, whereas the other 48 high-frequency components are processed as feature maps in the subsequent feature conversion layers. DLR with a separated path of high-frequency components can learn convolutional neural network parameters to remove noise and maintain detailed structures. After the denoising process, the denoised high-pass components (**d**) and the zero-frequency component (**e**) are combined

the CSF and pons was determined using the following formula: $CNR = (mean\ signal\ intensity_{CSF} - mean\ signal\ intensity_{pons}) / (mean\ standard\ deviation_{CSF})$.

Additionally, we compared the contralateral normal trigeminal nerve sharpness using full width at half maximum (FWHM) between the two types of 3D FASE images. We measured the FWHM value according to the signal intensity profile along a line crossing the trigeminal nerve in an axial image of HR-MR cisternography (Fig. 4).

Qualitative image analysis

Neuroradiologists without knowledge of individual subject characteristics and reconstructed images were selected to evaluate the two types of HR-MR cisternography images. Images were qualitatively assessed by two neuroradiologists with 11 and 7 years of experience evaluating MRI images. Noise quality, sharpness, and overall image quality in the two types of 3D FASE images were scored as follows: 1, poor; 2, fair; 3, good; and 4, excellent. Additionally, artifacts were scored as follows: 1, image not diagnostic because of artifacts; 2, major artifacts without diagnostic relevance; 3, minor artifacts; and 4, no artifacts.

Statistical analysis

Wilcoxon signed-rank tests were performed to compare the SNR, contrast, FWHM, and qualitative analysis findings between images with and without DLR. All statistical analyses were performed using EZR (Saitama Medical Center Jichi Medical University, Saitama, Japan), which is a graphical user interface for R (The R Foundation for Statistical Computing, Vienna, Austria). A p value < 0.01 was considered statistically significant.

Results

All HR-MR cisternography assessments were completed successfully. Quantitative and qualitative data are presented in Tables 1 and 2, respectively.

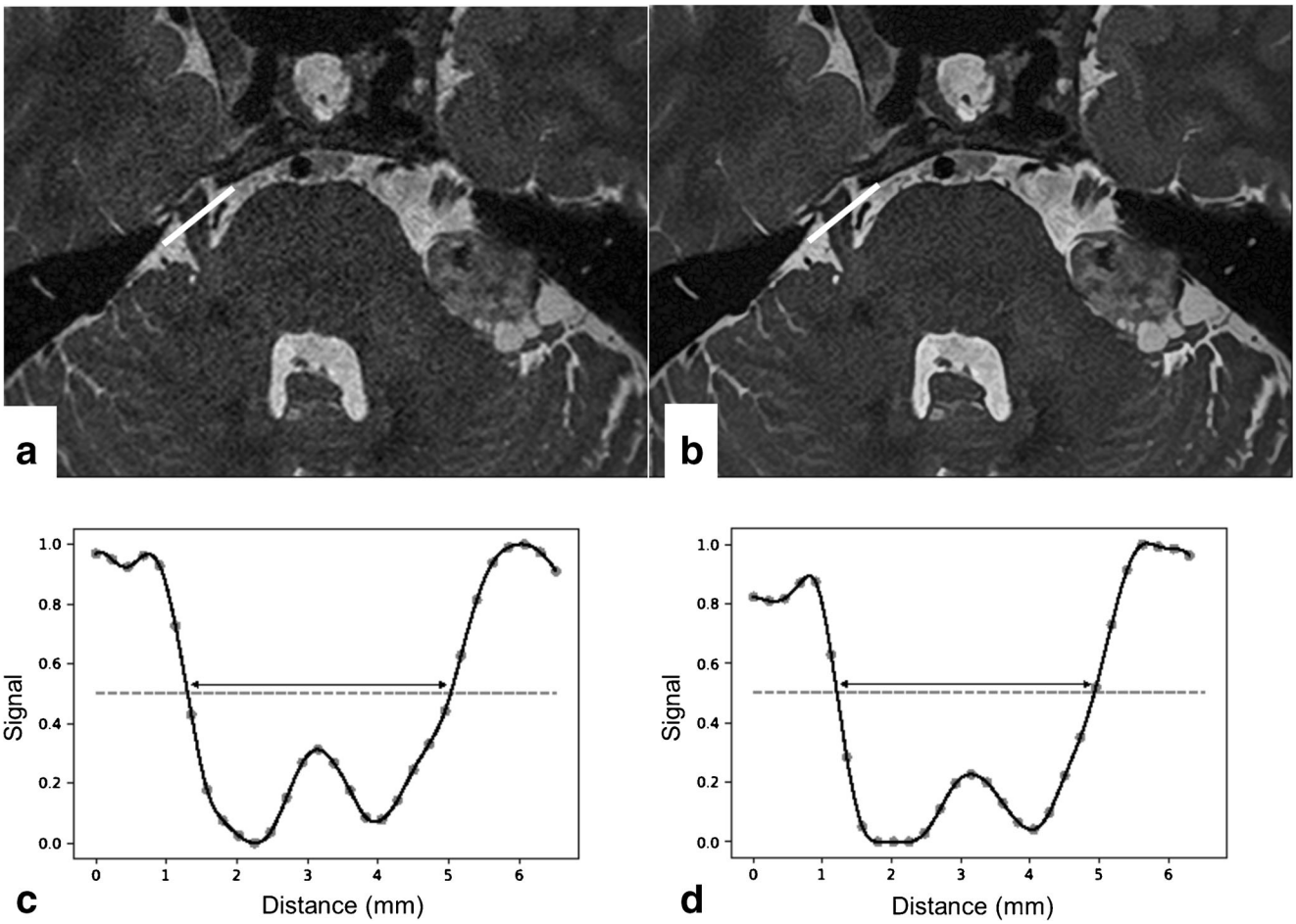

Fig. 4 Case of a man in his 40s with a left vestibular schwannoma. **a** Conventional reconstructed image without deep learning-based reconstruction (DLR); **b** reconstructed image with DLR; **c, d** profile curve along a line crossing the right trigeminal nerve. The arrow indicates full width at half maximum (FWHM). HR-MR cisternography shows a mass lesion with a cyst in the cerebellopontine angle. Image noise is lower and the signal-to-noise ratio (SNR) is higher with DLR than without DLR. The identification of small vessels near the tumor is superior with DLR than without DLR. FWHM in the profile curve is similar between with DLR and without DLR

Quantitative image analysis

The results of quantitative image analysis are shown in Table 1 and Fig. 5. The SNRs and CNRs of the CSF and pons were significantly higher with DLR than without DLR (SNR of CSF 21.81 ± 7.60 vs. 15.33 ± 4.03, $p < 0.001$; SNR of pons 5.96 ± 1.38 vs. 3.99 ± 0.48, $p < 0.001$; CNR 13.60 ± 7.41 vs. 11.13 ± 3.00, $p < 0.001$). However, there were no significant differences between without and with DLR in the contrast of the CSF and pons (0.54 ± 0.03 vs. 0.55 ± 0.03, $p = 0.225$) and the sharpness of the normal-side trigeminal nerve using FWHM (3.50 ± 4.11 vs. 3.51 ± 0.77; $p = 0.185$).

Table 1 Results of quantitative assessments

		Conventional without DLR	DLR	*p*
SNR	CSF	15.33 ± 4.03	21.81 ± 7.60	< 0.001
	Pons	3.99 ± 0.48	5.96 ± 1.38	< 0.001
Contrast ratio		0.54 ± 0.03	0.55 ± 0.03	0.225
CNR		11.13 ± 3.00	13.60 ± 7.41	< 0.001
FWHM		3.50 ± 4.11	3.51 ± 0.77	0.185

SNR signal-to-noise ratio
FWHM full width at half maximum
DLR deep learning reconstruction
CNR contrast-to-noise ratio

Table 2 Results of qualitative assessments

	Conventional without DLR	DLR	*p*
Noise quality	2.53 ± 0.44	3.95 ± 0.19	< 0.001
Image sharpness	3.03 ± 0.17	3.07 ± 0.25	0.371
Artifact	2.94 ± 0.24	2.97 ± 0.17	1
Overall image quality	2.97 ± 0.12	3.97 ± 0.17	< 0.001

DLR deep learning reconstruction

Qualitative image analysis

The results of quantitative image analysis are shown in Table 2. Representative cases are shown in Figs. 4 and 6. Noise quality and the overall image quality were significantly higher with DLR than without DLR (noise quality 3.95 ± 0.19 vs. 2.53 ± 0.44, $p < 0.001$; overall image quality 3.97 ± 0.17 vs. 2.97 ± 0.12, $p < 0.001$). There were no significant differences between without and with DLR in sharpness (3.07 ± 0.25 vs. 3.03 ± 0.17, $p = 0.371$) and artifacts (2.97 ± 0.17 vs. 2.94 ± 0.24, $p = 1$).

Discussion

Our results demonstrated that DLR increased the SNR and CNR without sacrificing spatial resolution in HR-MR cisternography. In qualitative assessment, noise quality was significantly higher with DLR than without DLR. However, there was no significant difference in image sharpness.

Some image denoising methods for MRI do not preserve spatial resolution, and they result in image blurring. MR signals contain various noises and artifacts, and generally, two basic methods have been used for image denoising (filtering method and transform method). The filtering method involves the adoption of image filters, such as average, median, Gaussian, adaptive mean/median, principal component analysis based, and non-local means filters [24, 25]. These image filters remove noise without any attempt to explicitly identify it by performing a kind of low-pass filtering on groups of pixels with the assumption that noise is present in the higher region of the frequency spectrum. The Fourier transform method, which is a major transform method, in MRI also involves a kind of low-pass filtering in the frequency domain (k-space) with a cutoff frequency on the basis that noise components are de-correlated from the useful signal in the frequency domain [26]. Recently, another transform method called wavelet transform has been widely used mainly for compressed sensing. The standard Fourier transform method localizes only the frequency components, whereas the wavelet transform method localizes both time and frequency components [27, 28]. The wavelet transform method is more useful than the Fourier transform method because it can be applied to non-stationary signals as medical images are only piecewise smooth and noise distributions are random in nature. However, the wavelet transform method also reduces noise by removing high-frequency components of images according to predefined rules, and it has been reported that blurring occurs even with this method. This is not a serious problem for non-HR MRI; however, it is a serious problem for HR MRI because the rate of high-frequency objects increases.

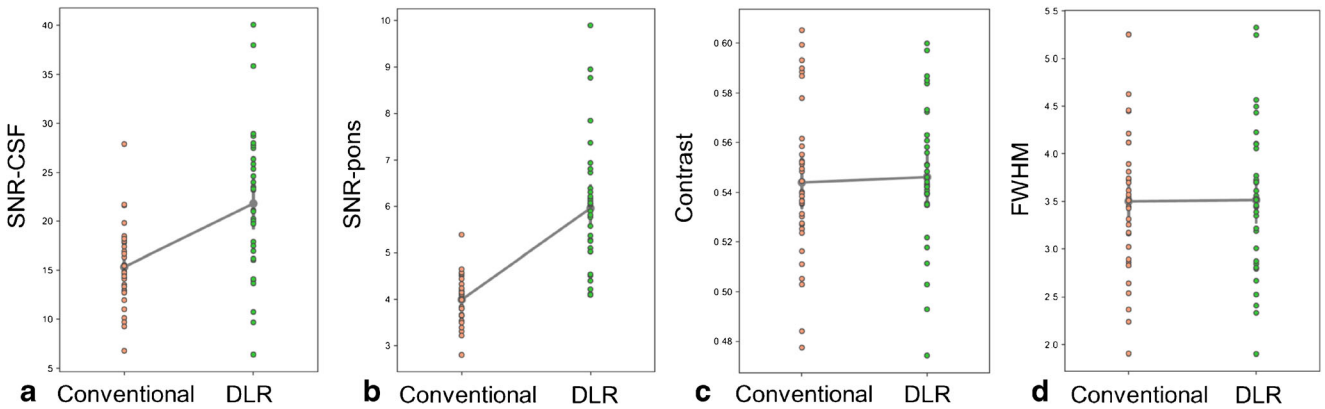

Fig. 5 Quantitative assessments. **a** Signal-to-noise ratio (SNR)-CSF; **b** SNR-pons; **c** contrast; **d** full width at half maximum (FWHM). The SNRs of the CSF and pons are significantly higher with deep learning-based reconstruction (DLR) than without DLR. There are no significant differences between without and with DLR in the contrast of the CSF and pons and the sharpness of the normal-side trigeminal nerve using FWHM

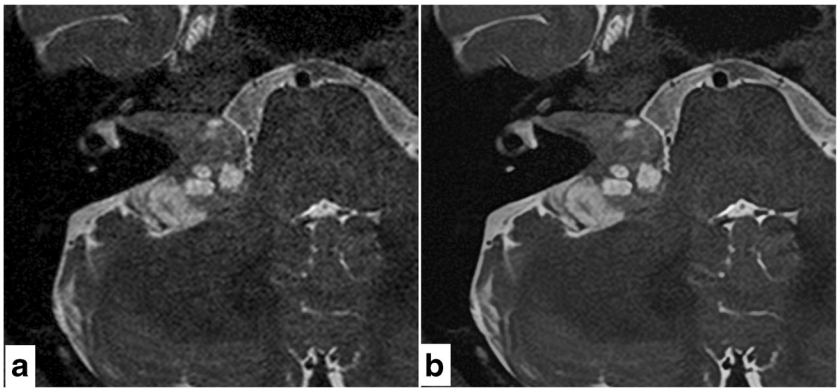

Fig. 6 Case of a woman in her 60s with a right vestibular schwannoma. **a** Conventional reconstructed image without deep learning-based reconstruction (DLR); **b** reconstructed image with DLR. HR-MR cisternography shows a mass lesion with a cyst extending from the right internal auditory canal to the cerebellopontine angle. Identifications of the cerebellopontine angle, internal auditory canal tumor structure, and small vessels near the tumor are superior with DLR than without DLR

We found that DLR could decrease image noise without sacrificing spatial resolution in HR-MR cisternography. Deep learning approaches for image noise reduction differ greatly from non-machine learning methods in that they can learn the pattern of anatomical structures and image noise from training data. Our DLR method aimed to remove only noise with preservation of the comprehensive structure by learning various noises with training image pairs of a high-SNR image and a noisy input image. As a specific procedure, input data were divided into a high-frequency domain and low-frequency domain, and the method was trained to generate noise-less data from noise-containing data in the high-frequency domain [20]. The adoption of a learning process specialized for the high-frequency domain might be the reason why our DLR method can maintain the edges of anatomical structures. Another advantage of this approach is that MRI contrast is concentrated in the low-frequency domain; thus, this method might be easily applied to other sequences. In addition, current DLR techniques can be used with wavelet denoising techniques in principle, and better denoising can be possible using a combination of the two techniques in the future. The merits of the DLR denoising technique used in current study include the following: (1) the ability to reduce only noise signals with preservation of the comprehensive structure by learning various noise signal, (2) application to many sequences (e.g., T1WI, T2WI, FLAIR images, proton-density-weighted images, and diffusion-weighted images) and any part of the body; (3) in principle to be used in combination with wavelet denoising techniques, and (4) easily implemented by many facilities because this technique is commercially available. Limitations of this technique are following: (1) It is not possible to depict small structures that are not detected in the original images; (2) it has not been adequately validated because of the state-of-the-art technique; and (3) it is impossible to reduce artifacts (e.g., motion artifacts and magnetic susceptibility artifacts) except for the Gaussian noise.

The present study has several limitations. First, this study was designed to evaluate the image quality of DLR in HR-MR cisternography, and the diagnostic performance of DLR was not evaluated. Second, we did not compare DLR images with high number of excitation images without DLR. However, scanning two long sequences might be uncomfortable and might increase the rate of a poor study, and it could raise ethical issues. Third, the small size of our study population and the limited scope of the dataset, including the use of a single scanner source, might limit the generalization of our findings. Fourth, the scan time of HR 3D T2WIs used in our study was slightly long. We could not use commercial-based compressed sensing technique in this study. It was necessary to acquire 3D HR T2WIs with high spatial resolution because we had to assess the relationship between the cerebellopontine tumor and cranial nerves (such as the facial, cochlear, and vestibular nerves) in detail. Fifth, we could not reconstruct using different DLRs without high-frequency domain because we used a vendor-specific denoising method. We think that it may be necessary to compare our method with other vendors' methods. Finally, we did not compare DLR and the state-of-the-art denoising technique of compressed sensing because our MRI scanner was not capable of HR-MR cisternography with compressed sensing. It may be necessary to compare the DLR technique with the compressed sensing technique in future research.

Conclusion

DLR can improve the image quality of HR-MR cisternography by reducing image noise without sacrificing contrast or sharpness.

Authors' contributions All authors contributed to the study conception and design. Material preparation, data collection, and analysis were performed by Hiroyuki Uetani, Tadashi Hamasaki, Machiko Tateishi,

Kosuke Morita, Akira Sasao, and Seitaro Oda. The first draft of the manuscript was written by Hiroyuki Uetani, and all authors commented on the previous versions of the manuscript. All authors read and approved the final manuscript.

Conceptualization: Hiroyuki Uetani and Takeshi Nakaura

Data collection: Hiroyuki Uetani, Tadashi Hamasaki, Machiko Tateishi, Kosuke Morita, Akira Sasao, and Seitaro Oda

Methodology: Hiroyuki Uetani, Takeshi Nakaura, Mika Kitajima, and Yuichi Yamashita

Formal analysis and investigation: Hiroyuki Uetani, Takeshi Nakaura, Mika Kitajima, and Machiko Tateishi

Writing—original draft preparation: Hiroyuki Uetani

Writing—review and editing: Takeshi Nakaura, Mika Kitajima, Osamu Ikeda, and Yasuyuki Yamashita

Supervision: Takeshi Nakaura, Mika Kitajima, Osamu Ikeda, and Yasuyuki Yamashita

Funding information None.

Compliance with ethical standards

Conflict of interest Yuichi Yamashita is an employee of Canon Medical Systems. The other authors declare that they have no conflicts of interest.

Ethical approval All procedures followed the clinical study guidelines of the ethics committee of Kumamoto university hospital (Kumamoto, Japan), and they were approved by our institutional review board.

Informed consent For this type of study, formal consent is not required.

References

1. Naganawa S, Koshikawa T, Fukatsu H, Ishigaki T, Fukuta T (2001) MR cisternography of the cerebellopontine angle: comparison of three-dimensional fast asymmetrical spin-echo and three-dimensional constructive interference in the steady-state sequences. AJNR Am J Neuroradiol 22:1179–1185
2. Liu P, Saida Y, Yoshioka H, Itai Y (2003) MR imaging of epidermoids at the cerebellopontine angle. Magn Reson Med Sci 2:109–115
3. Masuda Y, Yamamoto T, Akutsu H, Shiigai M, Masumoto T, Ishikawa E, Matsuda M, Matsumura A (2015) Usefulness of subtraction of 3D T2WI-DRIVE from contrast-enhanced 3D T1WI: preoperative evaluations of the neurovascular anatomy of patients with neurovascular compression syndrome. AJNR Am J Neuroradiol 36:317–322
4. Nowe V, De Ridder D, Van de Heyning PH, Wang XL, Gielen J, Van Goethem J, Ozsarlak O, De Schepper AM, Parizel PM (2004) Does the location of a vascular loop in the cerebellopontine angle explain pulsatile and non-pulsatile tinnitus? Eur Radiol 14:2282–2289
5. Ryu H, Tanaka T, Yamamoto S, Uemura K, Takehara Y, Isoda H (1999) Magnetic resonance cisternography used to determine precise topography of the facial nerve and three components of the eighth cranial nerve in the internal auditory canal and cerebellopontine cistern. J Neurosurg 90:624–634
6. Hentschel MA, Kunst HPM, Rovers MM, Steens SCA (2018) Diagnostic accuracy of high-resolution T2-weighted MRI vs contrast-enhanced T1-weighted MRI to screen for cerebellopontine angle lesions in symptomatic patients. Clin Otolaryngol 43:805–811
7. Gamaleldin OA, Donia MM, Elsebaie NA, Abdelkhalek Abdelrazek A, Rayan T, Khalifa MH (2020) Role of fused three-dimensional time-of-flight magnetic resonance angiography and 3-dimensional T2-weighted imaging sequences in neurovascular compression. World Neurosurg 133:e180–e186
8. Kanoto M, Toyoguchi Y, Hosoya T, Oda A, Sugai Y (2013) Visualization of the trochlear nerve in the cistern with use of high-resolution turbo spin-echo multisection motion-sensitized driven equilibrium. AJNR Am J Neuroradiol 34:1434–1437
9. Aja-Fernandez S, Vegas-Sanchez-Ferrero G, Tristan-Vega A (2014) Noise estimation in parallel MRI: GRAPPA and SENSE. Magn Reson Imaging 32:281–290
10. Pruessmann KP, Weiger M, Scheidegger MB, Boesiger P (1999) SENSE: sensitivity encoding for fast MRI. Magn Reson Med 42:952–962
11. Monch S, Sollmann N, Hock A, Zimmer C, Kirschke JS, Hedderich DM (2019) Magnetic resonance imaging of the brain using compressed sensing - quality assessment in daily clinical routine. Clin Neuroradiol 30:279–286. https://doi.org/10.1007/s00062-019-00789-x
12. Zhang T, Chowdhury S, Lustig M, Barth RA, Alley MT, Grafendorfer T, Calderon PD, Robb FJ, Pauly JM, Vasanawala SS (2014) Clinical performance of contrast enhanced abdominal pediatric MRI with fast combined parallel imaging compressed sensing reconstruction. J Magn Reson Imaging 40:13–25
13. Sharma SD, Fong CL, Tzung BS, Law M, Nayak KS (2013) Clinical image quality assessment of accelerated magnetic resonance neuroimaging using compressed sensing. Investig Radiol 48:638–645
14. Chilamkurthy S, Ghosh R, Tanamala S, Biviji M, Campeau NG, Venugopal VK, Mahajan V, Rao P, Warier P (2018) Deep learning algorithms for detection of critical findings in head CT scans: a retrospective study. Lancet 392:2388–2396
15. Ueda D, Yamamoto A, Nishimori M, Shimono T, Doishita S, Shimazaki A, Katayama Y, Fukumoto S, Choppin A, Shimahara Y, Miki Y (2019) Deep learning for MR angiography: automated detection of cerebral aneurysms. Radiology 290:187–194
16. Perkuhn M, Stavrinou P, Thiele F, Shakirin G, Mohan M, Garmpis D, Kabbasch C, Borggrefe J (2018) Clinical evaluation of a multiparametric deep learning model for glioblastoma segmentation using heterogeneous magnetic resonance imaging data from clinical routine. Investig Radiol 53:647–654
17. Lin L, Dou Q, Jin YM, Zhou GQ, Tang YQ, Chen WL, Su BA, Liu F, Tao CJ, Jiang N, Li JY, Tang LL, Xie CM, Huang SM, Ma J, Heng PA, Wee JTS, Chua MLK, Chen H, Sun Y (2019) Deep learning for automated contouring of primary tumor volumes by MRI for nasopharyngeal carcinoma. Radiology 291:677–686
18. Dunnmon JA, Yi D, Langlotz CP, Ré C, Rubin DL, Lungren MP (2019) Assessment of convolutional neural networks for automated classification of chest radiographs. Radiology 290:537–544
19. Wang H, Zhang J, Bao S, Liu J, Hou F, Huang Y, Chen H, Duan S, Hao D, Liu J (2020) Preoperative MRI-based radiomic machine-learning nomogram may accurately distinguish between benign and malignant soft-tissue lesions: a two-center study. J Magn Reson Imaging. https://doi.org/10.1002/jmri.27111
20. Jiang D, Dou W, Vosters L, Xu X, Sun Y, Tan T (2018) Denoising of 3D magnetic resonance images with multi-channel residual learning of convolutional neural network. Jpn J Radiol 36:566–574
21. Zhang K, Zuo W, Chen Y, Meng D, Zhang L (2017) Beyond a Gaussian denoiser: residual learning of deep CNN for image denoising. IEEE Trans Image Process 26:3142–3155
22. Kidoh M, Shinoda K, Kitajima M, Isogawa K, Nambu M, Uetani H, Morita K, Nakaura T, Tateishi M, Yamashita Y, Yamashita Y (2019) Deep learning based noise reduction for brain MR imaging: tests on phantoms and healthy volunteers. Magn Reson Med Sci 19:195–206. https://doi.org/10.2463/mrms.mp.2019-0018

23. Isogawa K, Ida T, Shiodera T, Takeguchi T (2018) Deep shrinkage convolutional neural network for adaptive noise reduction. IEEE Signal Process Lett 25:224–228
24. Erturk MA, Bottomley PA, El-Sharkawy AM (2013) Denoising MRI using spectral subtraction. IEEE Trans Biomed Eng 60: 1556–1562
25. Sijbers J, den Dekker AJ, Van der Linden A, Verhoye TM, Van Dyck D (1999) Adaptive anisotropic noise filtering for magnitude MR data. Magn Reson Imaging 17:1533–1539
26. Donoho DL (1995) De-noising by soft-thresholding. IEEE Trans Inf Theory 41:613–627
27. Laine AF (2000) Wavelets in temporal and spatial processing of biomedical images. Annu Rev Biomed Eng 2:511–550
28. Yang X, Fei B (2011) A wavelet multiscale denoising algorithm for magnetic resonance (MR) images. Meas Sci Technol 22:25803